Experiments on the Richtmyer–Meshkov instability: Small-scale perturbations on a plane interface

M. Brouillette[a] and B. Sturtevant
Graduate Aeronautical Laboratories, California Institute of Technology, Pasadena, California 91125

(Received 10 September 1991; accepted 1 December 1992)

This paper reports the results of measurements of the "visual thickness," obtained from flow visualization experiments by the schlieren method, of initially plane interfaces between two gases under impulsive accelerations. It is found that when such interfaces are processed by just one incident shock wave of strength of order $M_s=1.5$, their thickness increases slowly and they require observation over extended times; their growth rates are found to slow down with time, in agreement with simple theoretical arguments. The observed growth rates of thin interfaces formed by plastic membranes have been found to be substantially smaller than that reported by previous investigators. Also, thick, diffusively smoothed interfaces initially grow much more slowly than the discontinuous ones do. In these experiments, it is found that wall vortices formed by shock wave/boundary-layer interaction at the interface grow much more rapidly than the shock-processed interfaces in the bulk of the fluid. These wall structures can reduce the apparent growth of interfaces by vorticity-induced strain and impair the observation of the relevant interface phenomena.

I. INTRODUCTION

The refraction of a shock wave from an interface between two fluids of different densities causes the distortion of any perturbation initially present on the interface. This class of problems is known as the Richtmyer–Meshkov instability.[1,2] As the interface between the two fluids distorts, nonlinear processes take place and a region of turbulence develops, resulting in the mixing of the two fluids. The arrival of any additional pressure waves at the interface further increases the intensity of the turbulent motions. Turbulent mixing between the two impulsively accelerated fluids can be considered beneficial, in supersonic and hypersonic combustion applications,[3,4] for example, or deleterious, such as in inertial confinement fusion experiments.[5,6]

Experiments to observe the turbulent mixing at a plane smooth interface between gases of different densities under shock acceleration have been performed in the Soviet Union,[7–9] France,[10] and the United States,[11] among others. In this case, the seeds for the development of a turbulent mixing zone (TMZ) between the two fluids are only the random small-scale perturbations initially present at the interface and those introduced by experimental artifacts. Our first series of experiments[12] has focused on the development of the TMZ at the interface as it is repeatedly processed by reflections of the primary shock wave reverberating between the end wall of the shock tube and the interface. It was found that, since the growth rates are small for these and most laboratory-scale experiments, care must be taken to distinguish effects introduced by the experimental apparatus, including acoustic noise and shock wave/boundary-layer interaction, from the primary mechanisms under study. For example, the interaction of reverberations with the distorted interface within the boundary layer can cause the formation of a powerful wall vortex (cf. Fig. 1) which hinders the observation of interface phenomena in the bulk of the fluid and leads to an incorrect interpretation of the data if not properly taken into account.

This paper presents the results of a second series of experiments examining in detail the development of the TMZ after the interaction of a single shock wave and its first reverberation with a nominally flat interface between two gases of different densities. Experiments are performed with thin (discontinuous) and thick (continuous) interfaces, and both light–heavy and heavy–light gas combinations are considered; the visual thickness of the interface region is obtained from flow visualization by the schlieren method. It is found that the growth rate of the interface slows down with time, in agreement with simple theoretical arguments. Thick interfaces grow much more slowly than the thinner ones, which in turn exhibit substantially slower growth than reported by previous investigators. The growth rate of thick interfaces seems to be due more to perturbations introduced during the experiment than to inhomogeneities initially present in the interfacial gas; they therefore require observation over extended times. Because the development of the instability at the interface depends directly on the nature of the perturbation on it, it is not certain whether the turbulent mixing zone ever achieves a stage of self-similar development independent of initial conditions. It is found that correlations from gravitational mixing experiments overpredict the thickening rate of the interface.

II. THEORETICAL CONSIDERATIONS

For applications in which the interfaces are made as smooth as possible and the configurations are arranged with the shocks parallel to the interfaces, the wavelength λ and amplitude η of the perturbations are small. According

[a]Present address: Département de Génie Mécanique, Université de Sherbrooke, Sherbrooke, Québec J1K 2R1, Canada.

 0899-8213/93/040916-15$06.00

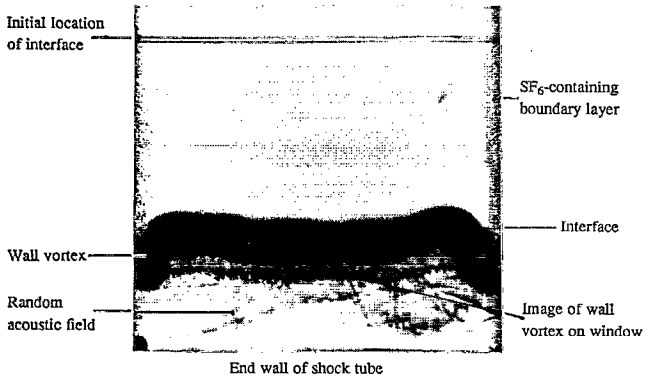

FIG. 1. Spark schlieren photograph of the Richtmyer–Meshkov instability of a plane continuous interface between air (above) and SF_6 (below). $M_s=1.32$, $t=1.91$ msec, short period configuration. The interface, now stationary, is shown after the reverberations of the primary wave between the interface and the end wall of the shock tube have decayed. The interface thickness has not yet grown from the beginning of the experiment. (From Fig. 12 of Ref. 12.)

to the linear theory of Richtmyer,[1] small-scale perturbations grow rapidly into the nonlinear regime $\eta \approx \lambda$, and the refraction of the shock from the interface generates small-scale turbulence by the baroclinic vorticity production mechanism. Merging of the scales associated with the fluid motion and entrainment by the resulting large-scale structures then become the dominant mechanisms for mixing at the interface. Qualitative numerical evidence for this scenario was obtained by Mikaelian[13] where the emergence of large-scale structures from the initially small-scale fluctuations was observed.

The total kinetic energy per unit area E_k deposited at a discontinuous interface by the Richtmyer–Meshkov instability can be obtained from the linear theory as

$$E_k=\frac{1}{2}\bar{\rho}\frac{2\pi}{\lambda}[u]^2A'^2\eta_0'^2, \tag{1}$$

where A is the Atwood ratio based on the fluid densities across the interface ρ_1 and ρ_2, respectively, $A\equiv(\rho_2-\rho_1)/(\rho_1+\rho_2)$, $\bar{\rho}=(\rho_1+\rho_2)/2$ is the average density across the interface, $[u]$ is the interface velocity change induced by the shock wave, and η_0 is the initial amplitude of the perturbation. The primes denote the use of postshock refraction properties, as prescribed by Richtmyer[1] and Sturtevant.[14] Saffman and Meiron[15] have shown that the kinetic energy production is decreased when the density gradient at the interface is reduced. In any case, part of this energy is available for the turbulent motions and ultimately all of it is dissipated into heat by the action of viscosity. The total kinetic energy thus depends on the initial configuration of the interface through $\eta_0'^2/\lambda$. Considering the influence of initial conditions on the energy available for the turbulent motions at the impulsively accelerated interface, and the fact that no additional energy is created after the refraction of the incident shock, it seems doubtful that the development of the turbulence achieves a self-similar regime independent of initial conditions, as is well documented for the constant gravity experiments.[16]

Furthermore, for the impulsive case, since the energy responsible for the fluid motions is deposited at the interface only at the time of the impulsive acceleration, the turbulence intensity decays in time due to the thickening of the interface region, the action of viscosity, and the possible radiation of wave energy. We have discussed the time evolution of the thickness δ of the TMZ in previous publications.[12,17] These arguments can be summarized as follows.

For small time t the flow develops conically in space-time,

$$\frac{\delta}{[u]t}=f(A', IC, M), \tag{2}$$

where A' is the postshock Atwood ratio defined above, IC represent the initial conditions, and M the interface Mach number, i.e., compressibility effects; f is a functional dependence to be determined. Equation (2) simply states that, initially, the TMZ should grow linearly with time. Later, as the thickness of the TMZ increases, the turbulence intensity decreases since the turbulent kinetic energy is distributed over a larger volume. At later times, $\delta \propto t^{\alpha}$, where $\alpha=2/3$ in the absence of viscous stress; when viscous dissipation is taken into account, $\alpha<2/3$ and is dependent on the choice of turbulence model.[18] The time t^* at which transition from the linear to the power-law regime occurs can be estimated for the inviscid case by patching the two solutions using simple arguments involving the conservation of energy at the interface. It can be shown[17] that the transition time goes as $t^* \propto E_k^{-1/2} \propto [u]^{-1}$. The linear portion of the interface evolution is shortened as the incident shock Mach number is increased; viscous dissipation further reduces the transition time.

Because of its complexity, the time evolution of the TMZ has so far been treated mostly by detailed numerical computation using turbulence closure models, e.g., by Andronov *et al.*[8] and Leith.[19] Due to the lack of experimental data for these flows, these models were tuned to results from constant-gravity experiments with liquids and to shear-driven turbulence experiments. However, with more experimental data becoming available for shock-driven flows, new numerical models are currently being developed.[20]

Mikaelian[21] adapted the constant-acceleration experimental results of Read[16] in a manner similar to the way in which Richtmyer[1] translated to the impulsive case the theory of Taylor[22] for the interface under gravitational acceleration. For the shock-induced turbulent thickening of an initially flat interface between two gases of different densities, he obtained the analytical result $\delta=0.28[u]A't$. We denote this expression as the Mikaelian–Read formula. Thus, for this case, the function f of Eq. (2) becomes $f=0.28A'$, and therefore is assumed independent of initial conditions and compressibility effects.

The effect of multiple wave interaction with the turbulent interface is an even more difficult problem. It is im-

portant to note that, even in the absence of the baroclinic instability at the interface, the passage of a shock wave through a turbulent region can lead to dramatically increased mixing simply by rapid distortion[23,24] and shock scattering.[25] The interaction of a shock with a region of highly nonisotropic turbulence is impossible to treat analytically since detailed information about the initial turbulent state is required. The tendency to return to isotropy may result in a smaller net enhancement of the turbulence. Finally, for strong incident shocks, these processes may inherently be compressible, and a significant amount of wave energy could be radiated from the interface.

III. EXPERIMENTAL FACILITY

A vertical shock tube has been built specially for the study of the shock-induced Rayleigh–Taylor instability. The test section, located at the bottom of the facility, incorporates a system to produce an interface between two gases of different densities. A shock wave is launched from the top of the shock tube toward the interface below. In the experiments reported here the interface is initially located near the end wall of the tube and the tube is set precisely vertical, so the development of mixing of two gases induced by an incident shock parallel to the interface, and its reverberations, is studied with schlieren photography. More details about the apparatus can be obtained from previous publications.[12,17]

We report here experiments with two different kinds of interfaces: (i) a conventional discontinuous interface formed by a thin plastic membrane and (ii) a thick membrane-free interface smoothed by molecular diffusion. The discontinuous interface is formed with a thin (0.5 μm) nitrocellulose membrane. It should be pointed here that the effect of membrane thickness and composition on the development of the shock-induced TMZ was not part of this investigation. Our laboratory has had good success with this type of membrane when they are made and cured properly. To form a continuous interface, the test section is also equipped with a system for withdrawing a thin (1.2 mm) horizontal metal plate initially separating the gases. With the light gas over the heavy one, the plate is withdrawn at a speed of 10 cm/sec, leaving a region of smooth density change between the two fluids.

For both types of interface, atmospheric air is used above the interface. Helium (He) (density 0.16 kg/m^3 at 25 °C, 1 atm), carbon dioxide (CO_2) (density 1.8 kg/m^3), Freon-22 (R22) (density 3.5 kg/m^3), and sulfur hexafluoride (SF_6) (density 6.0 kg/m^3), are used below the interface as test gases. With the present orientation of the shock tube, only light–heavy gas combinations are used with the sliding plate to form continuous interfaces. For this case we can vary the thickness of the continuous interface by increasing the delay between plate retraction and firing of the shock tube, which allows the gases to diffuse into each other.

To examine the turbulent thickening of the interface after interacting with a single shock wave, two experimental configurations are used: The initial development is studied with the interface initially in the field of view of the flow visualization windows (the so-called "short period" experiments). The late stages are investigated with the interface installed at two possible locations (32 cm or 65 cm) upstream of the windows ("long period" experiments). For the latter case, the end of the shock tube is adjusted to examine the interaction of the first reflection with the interface just as the latter is about to leave the window.

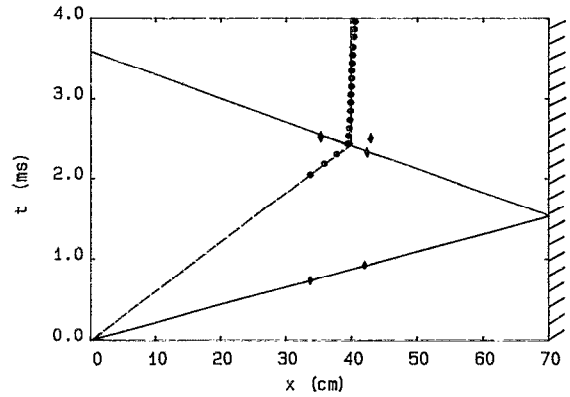

FIG. 2. Wave diagram for the interaction of a $M_s = 1.32$ shock wave with a nitrocellulose membrane, long period configuration. The interface trajectory is indicated by – – –: theory; ●: experiment. The wave trajectories are indicated by ——: theory; ♦: experiment.

The evolution of the interface under impulsive acceleration is observed using a schlieren optical system capable of taking high-resolution spark photographs or high-speed [35 000–60 000 frames per second (fps)] motion pictures. It is imperative to have the sensitivity of the schlieren system adjusted so that the interface can easily be distinguished from the image of the shock wave/boundary-layer interaction on the observing window to avoid an erroneous interpretation of the data.[12]

IV. WAVE DIAGRAMS

We present here selected experimental wave diagrams for the interaction of a shock wave with air–air, light–heavy, and heavy–light interfaces in the long period configuration. The data for this and subsequent wave diagrams were obtained from high-speed motion picture and pressure transducer records. The wave diagrams are compared to the simple one-dimensional gas-dynamics theory, which is also used to confirm the purity of the test gas. To obtain the origin of these wave diagrams, the observed time of arrival of the reflected shock at the interface is matched with the calculated value. The reader is referred to Ref. 12 for wave diagrams of experiments in the short period configuration, since their general features are the same as in the diagrams presented below.

A. Air–air discontinuous interface

Figure 2 shows the wave diagram for an air/air interface formed by a plastic membrane, impulsively accelerated by a $M_s = 1.32$ shock wave. The end wall is located 70 cm downstream of the initial position of the interface. A weak wave which might have been reflected from the mem-

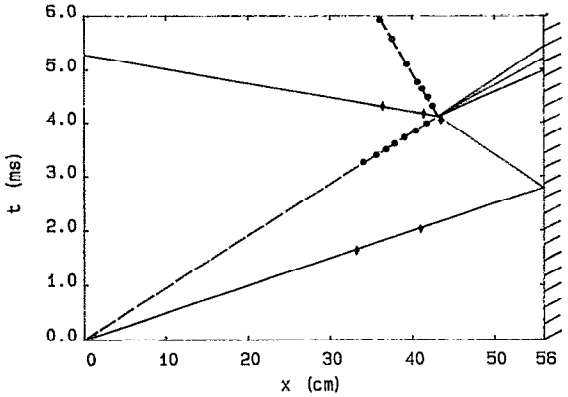

FIG. 3. Wave diagram for the interaction of a $M_s=1.32$ shock wave with a plane discontinuous interface between air and SF_6, long period configuration. The interface trajectory is indicated by – – –: theory; ●: experiment. The wave trajectories are indicated by ——: theory; ♦: experiment.

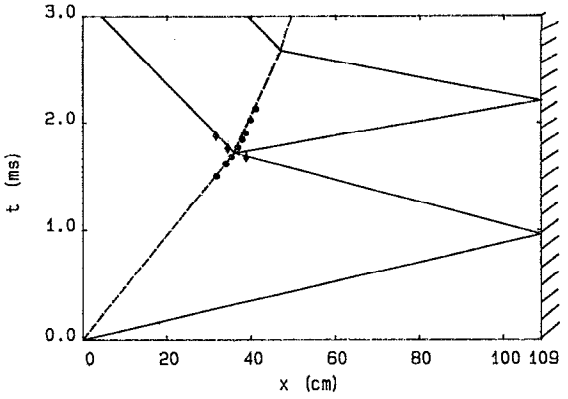

FIG. 4. Wave diagram for the interaction of a $M_s=1.32$ shock wave with a plane discontinuous interface between air and helium, long period configuration. The interface trajectory is indicated by – – –: theory; ●: experiment. The wave trajectories are indicated by ——: theory; ♦: experiment.

brane was not detected. At $t=1.53$ msec, the wave transmitted through the interface reflects from the end wall as a $M=1.29$ shock. At $t=2.47$ msec, this reflected shock (hereafter called the "reshock") interacts with the membrane, causing it to slow down almost to a stop. The reflected shock traverses the membrane and another weak wave is reflected back toward the end wall. By this point one-dimensional (1-D) gas-dynamics theory would predict that the reflected wave would bring the gases to rest. However, because the reflected shock accelerates the slowly moving gas in the boundary layer upwards, and, since on average the flow must be at rest, the air in the middle of the test section has to move downwards. Indeed the membrane is observed to proceed slowly down the tube, at a speed of 0.7 m/sec.

B. Light–heavy discontinuous interface

Figure 3 shows the wave diagram for an air/SF_6 interface accelerated by a $M_s=1.32$ shock wave. At $t=0$, the shock is incident at the interface, transmitting a $M=1.48$ shock into SF_6 and reflecting a $M=1.09$ shock in air. The transmitted shock reflects from the end wall at $t=2.79$ msec as a $M=1.46$ shock and interacts with the interface at $t=4.12$ msec. The interface then reverses its motion and expansion waves are reflected into SF_6. The agreement between the observed trajectories of the waves and the interface with familiar results from 1-D gas-dynamics theory is good. This suggests that the energy lost to the rupture of the membrane is negligible compared to that put in the motion of the gas. It would also seem to suggest that the presence of a density gradient at the interface reduces the adverse effects of the membrane on wave refraction, since better agreement is achieved between observed and calculated trajectories for the x-t diagram of air/SF_6 than for the air/air case.

C. Light–heavy continuous interface

Wave diagrams of experiments investigating the impulsive acceleration of a smooth transition between a light and a heavy gas are essentially the same as the one shown in Fig. 3. There is also good agreement with the 1-D gas-dynamics theory for the trajectory of the interface and waves.

D. Heavy–light discontinuous interface

Figure 4 shows the wave diagram for an air/He interface, accelerated by a $M_s=1.32$ shock wave. The main difference between this x-t diagram and that of Fig. 3 is that all reverberations are shocks, so the interface never reverses its motion but is gradually slowed down by the reshocks. There is good agreement between the observed shock and interface trajectories and those calculated from 1-D gas dynamics, indicating that there was no leakage through the membrane before this run.

V. VISUAL GROWTH OF TURBULENT MIXING ZONE

A. Air–air interfaces

A first step into the investigation of the development of discontinuous interfaces between gases of different densities is to perform experiments to study the time evolution of a nitrocellulose membrane after its impulsive acceleration by the incident shock and its first reverberation.

Figure 5 shows pictures obtained from a 35 000 fps schlieren motion picture of the interaction of an air/air interface with a $M_s=1.32$ shock wave, whose wave diagram was shown in Fig. 2. In Fig. 5(a) ($t=2.31$ msec), the membrane is seen as it traveled to the middle of the window. The membrane is still quite flat with small nonuniformities developing on its surface. The edges of the membrane are curved upwards and do not extend to the side walls due to the presence of the boundary layer, visible in the picture. It is believed that at this time the membrane is still intact in a single piece. The reflected shock can be seen at the bottom of the window. In Fig. 5(b) ($t=2.56$ msec), the reflected shock has just traversed the membrane and is traveling upward. The membrane has been slowed almost to a stop. The bifurcation of the reflected shock at the side

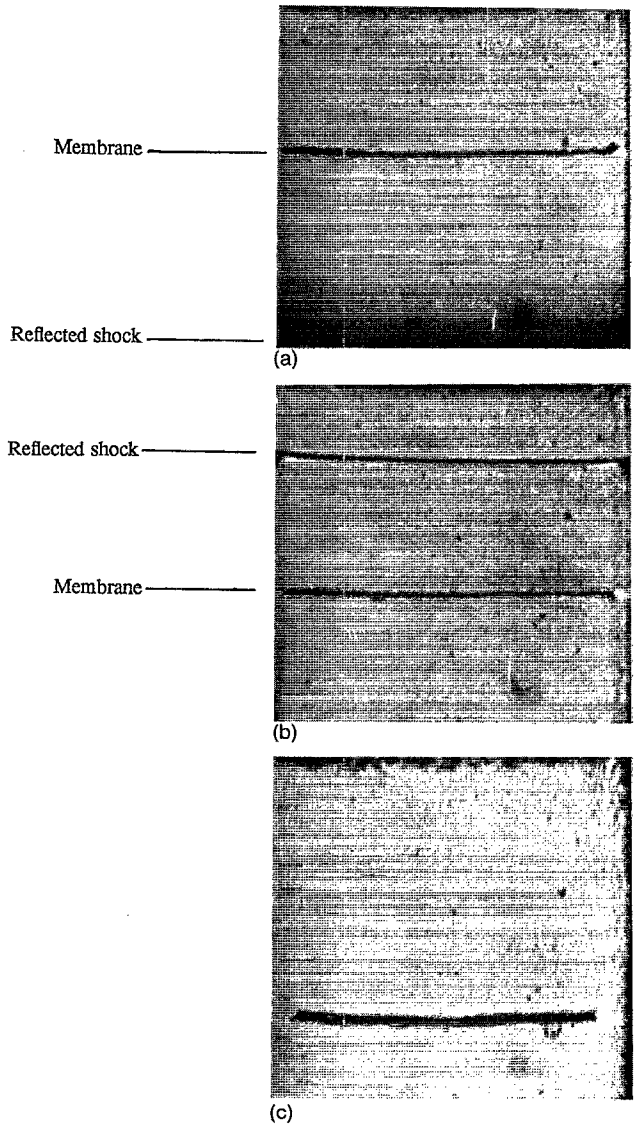

FIG. 5. Interaction of a nitrocellulose membrane with a $M_s=1.32$ shock wave, long period configuration. (a) $t=2.31$ msec, (b) $t=2.56$ msec, (c) $t=4.73$ msec.

walls can clearly be seen and is reminiscent of observations by Mark.[26] After the reshock, the membrane stays relatively flat and the gap at the side walls increases in size, perhaps due to erosion by the thickening boundary layer. In Fig. 5(c) ($t=4.73$ msec), the membrane has moved slightly toward the end of the tube, and some thickening of the interface region is observed probably due to the development of three-dimensional features. The membrane is still curved upwards and nonuniformities are more apparent.

Figure 6 shows a plot of the evolution of the thickness of the interface region formed by the distorted membrane in this experiment. The steplike nature of the data is due to the limited resolution of the measurements at these small thicknesses. The growth rate observed after the incident shock is negligible for the time interval the interface is within the observation window. Assuming that the initial

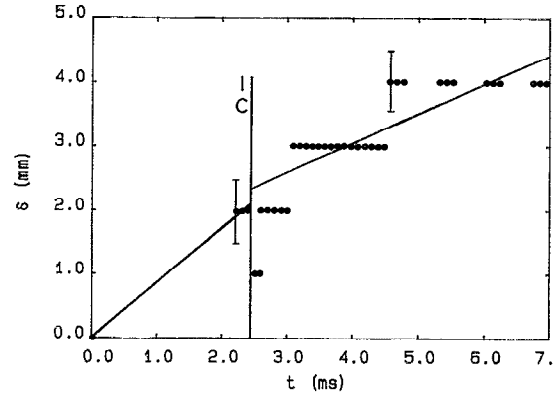

FIG. 6. Time evolution of the thickness of the interface region formed by the distorted membrane. $M_s=1.32$, long period configuration.

thickness is zero, the average growth rate from $t=0$ is calculated to be 0.9 ± 0.1 m/sec. After the reshock the apparent thickness increases at a rate of 0.5 ± 0.1 m/sec. Note that throughout, the rms deviation of straight-line least-squares fit of the data, indicated by straight solid lines in Figs. 6, 9, and subsequent plots for the time evolution of the thickness of the TMZ, is used to designate the bounds of the growth rate results. In these and subsequent plots, no attempt is made to distinguish departure from linear growth. Thus it can be seen that membrane perturbations still evolve after rupture, presumably due to a Richtmyer–Meshkov instability between the air and the membrane material.

Figures 7(a) and 7(b) show pictures of the air/air interface for incident shock Mach numbers 1.48 and 1.66, respectively. By comparing Figs. 5 and 7, it can be seen that, as the Mach number is increased, the interaction with the incident wave causes more membrane deterioration. The wrinkled shape of the membrane after rupture is demonstrated by the three-dimensional structure of the acoustic waves reflected by the membrane after the arrival of the reshock, as seen in Fig. 7(b) at $t=1.28$ msec. After corresponding late times, the membrane is also more deformed for strong incident waves.

It has been seen that a nitrocellulose membrane does not shatter in pieces after interaction with the incident shock wave, but translates down the shock tube at a velocity close to that predicted if the membrane were absent. This is because the membrane is initially very flat, so that there are few perturbations on the interface, and there is no density gradient across the interface, so that the Richtmyer–Meshkov instability across the interface is suppressed. However, because of flow obstruction by the membrane, there is a departure to the behavior predicted by the simple gas-dynamics theory after interaction with the first reshock.

B. Discontinuous interfaces

The time evolution of initially plane interfaces between gases of different densities under impulsive acceleration is presented in this section. The perturbations on the discon-

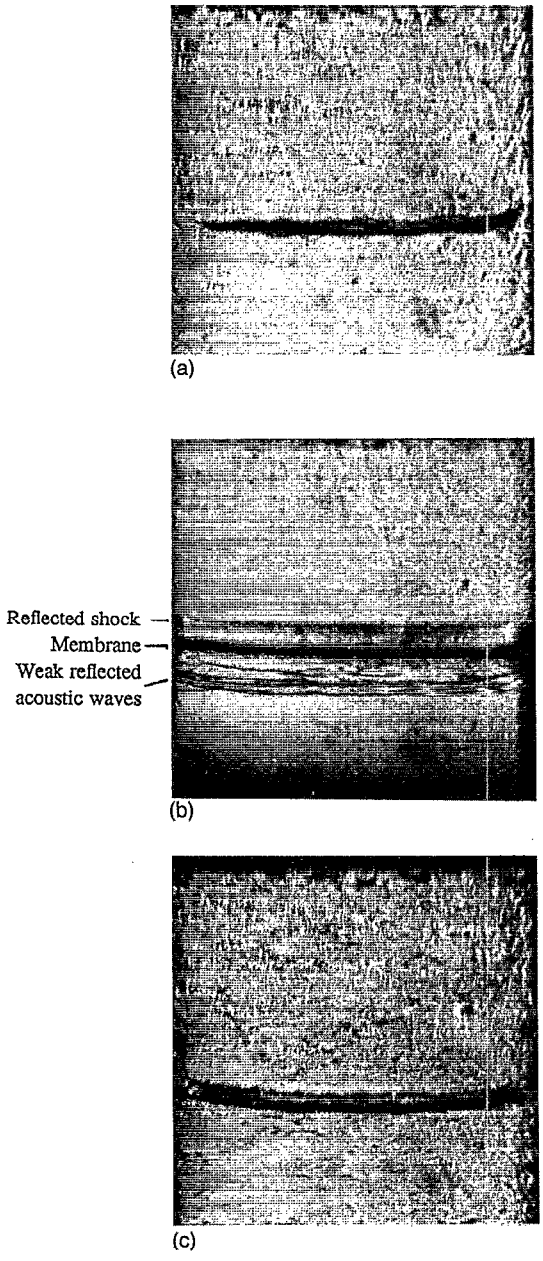

FIG. 7. Interaction of a nitrocellulose membrane with a shock wave, long period configuration. (a) $M_s=1.48$, $t=3.62$ msec; (b) $M_s=1.66$, $t=1.28$ msec; (c) $M_s=1.66$, $t=2.49$ msec.

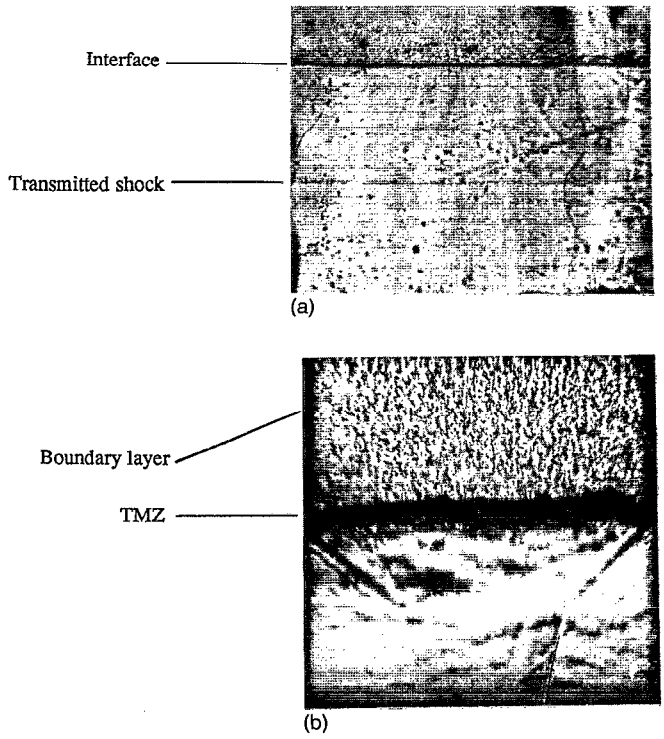

FIG. 8. Richtmyer–Meshkov instability of a plane discontinuous interface between air and SF_6. $M_s=1.32$, short period and long period configuration. (a) $t=0.34$ msec, (b) $t=3.59$ msec.

tinuous interface are introduced by the rupture of the supporting nitrocellulose membrane. It is found that, in this case, because of the large density gradient present at the interface, the membrane shatters in pieces that are subsequently entrained in the flow, as opposed to the air–air interfaces where the membrane appears to stay in one piece.

1. Growth after incident shock

To examine the time evolution of the TMZ at discontinuous interfaces after their interaction with the first incident shock, experiments were performed in both the long period and short period configurations. Experiments in the short period configuration, where the interface is initially just above the field of view of the flow visualization windows, allow the observation of the interface a short time after interaction with the incident shock. With the interface initially 32 cm (or 65 cm where noted) upstream of the windows, the experiments in the long period configuration allow the observation of the interface a long period after the arrival of the incident shock; an accurate determination of the average growth rate from $t=0$ is thus possible.

a. Light-heavy interface. Figure 8 shows frames taken from 35 000 fps motion pictures of the interaction of an air/SF_6 interface with a $M_s=1.32$ shock wave for both long period and short period experiments. The wave diagrams for those two runs were presented in Fig. 3 and Fig. 5 of Ref. 12. In Fig. 8(a), at $t=0.34$ msec, the interface is seen shortly after interaction with the incident shock. The interface appears flat, suggesting that any perturbations caused by the breaking of the membrane are small. The shock transmitted into SF_6 can be seen as it propagates toward the end wall at the bottom of the picture. The second photograph, taken $t=3.59$ msec after the arrival of the incident shock at the interface, shows the latter about halfway in the window. Turbulence is developing at the interface and is more apparent when compared with Fig. 8(a). The thick SF_6-rich boundary layer can be seen on the side walls above the interface.

Figure 9 is a plot of the evolution of the visual thickness δ of the TMZ for both short period and long period experiments. The thickness of the interface a short time

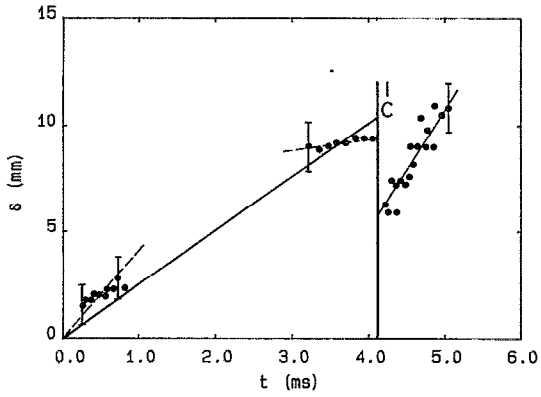

FIG. 9. Time evolution of the thickness of the TMZ for the plane discontinuous interface between air and SF_6. $M_s=1.32$, short period and long period configuration. ——: average incident shock growth, reshock growth. – – –: upper bound to early time growth, local incident shock growth.

after the interaction with the incident shock (obtained from the short period results) is so small that a fit to the data is not reliable enough to quote the incident shock growth rate for this time interval. However, an upper bound can be established at 3.8 m/sec as shown in the figure. The growth rate measured while the interface is in the field of view of the windows for the long period experiment, i.e., the so-called local growth rate, is only 1.0 ± 0.3 m/sec. Finally, the average growth rate from $t=0$ to the time of reshock is 2.3 ± 0.1 m/sec. It should be noted that the thickness of the simple laminar molecular diffusion layer between air and SF_6 would be less than 1 mm at the time of the reshock, as opposed to an observed TMZ thickness of 9 mm.

b. Heavy–light interface. Figure 10 shows frames obtained from 60 000 fps high-speed schlieren motion pictures of the interaction of an air/helium interface with a $M_s=1.30$ shock wave in the short period configuration, and with a $M_s=1.32$ shock in the long period configuration. The wave diagrams of those two experiments were presented in Fig. 4 and Fig. 8 of Ref. 12. In Fig. 10(a), taken 0.10 msec after the arrival of the incident shock, not much growth is observed since the beginning of the interaction. The second one, taken 1.55 msec after the arrival of the incident shock, shows the interface still traveling downwards. The fine-scale structure in the interface region suggests that turbulence is present. The thick helium-rich boundary layer is clearly seen on the side walls and on the window above the interface. A "toe" of helium under the air boundary layer is also visible, especially on the left side wall. As is often observed for the air/helium interfaces, fragments of nitrocellulose, probably ejected during rupture of the membrane, are convected ahead of the interface and are more visible in this case near the right side wall.

Figure 11 is a combined plot of the evolution of the TMZ after the interaction with the incident shock for these experiments. The upper bound to the growth measured in the short period configuration is 12.6 m/sec and the growth rate measured while the interface is in the field of

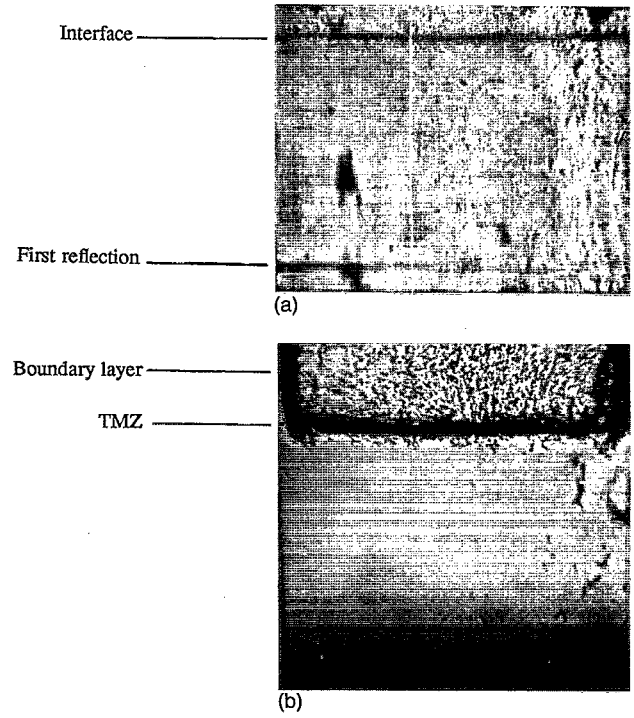

FIG. 10. Richtmyer–Meshkov instability of a plane discontinuous interface between air and helium, short period and long period configurations. (a) $M_s=1.30$, $t=0.10$ msec; (b) $M_s=1.32$, $t=1.55$ msec.

view of the windows in the long period configuration is 0.4 ± 0.1 m/sec. The average growth from $t=0$ to the time of first reshock is 3.3 ± 0.2 m/sec. Note that a laminar diffusion layer between the two gases would only be about 1 mm thick at the time of the reshock, as opposed to an observed TMZ thickness of 5.5 mm.

2. Growth after first reshock

The development of the TMZ after the arrival of the first reflection of the primary wave is examined in detail with experiments in the long period configuration.

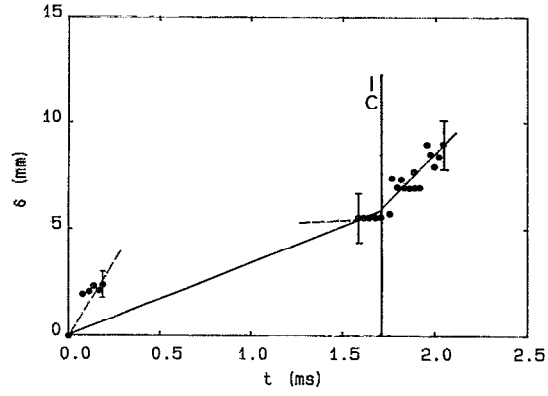

FIG. 11. Time evolution of the thickness of the TMZ for the plane discontinuous interface between air and helium. $M_s=1.32$, short period and long period configurations. ——: average incident shock growth, reshock growth. – – –: upper bound to early time growth, local incident shock growth.

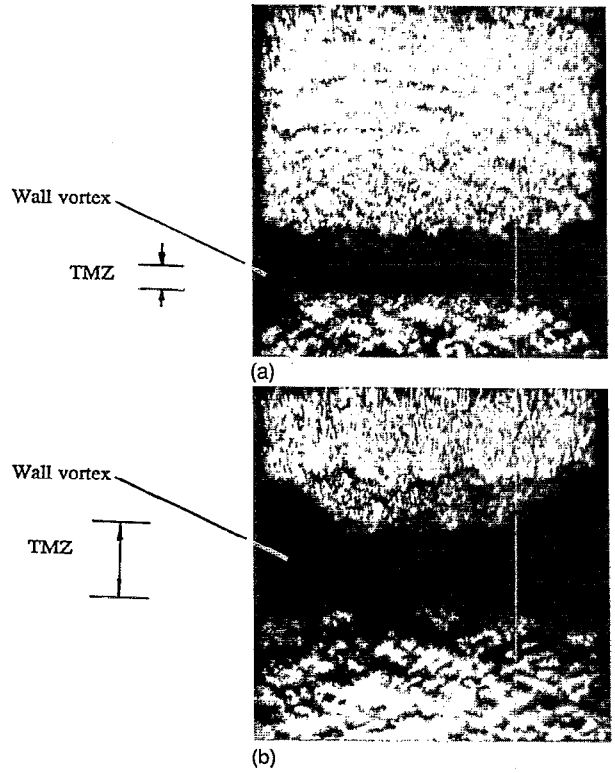

FIG. 12. Richtmyer–Meshkov instability of a plane discontinuous interface between air and SF_6. $M_s=1.32$, long period configuration. (a) $t=4.39$ msec, (b) $t=5.19$ msec.

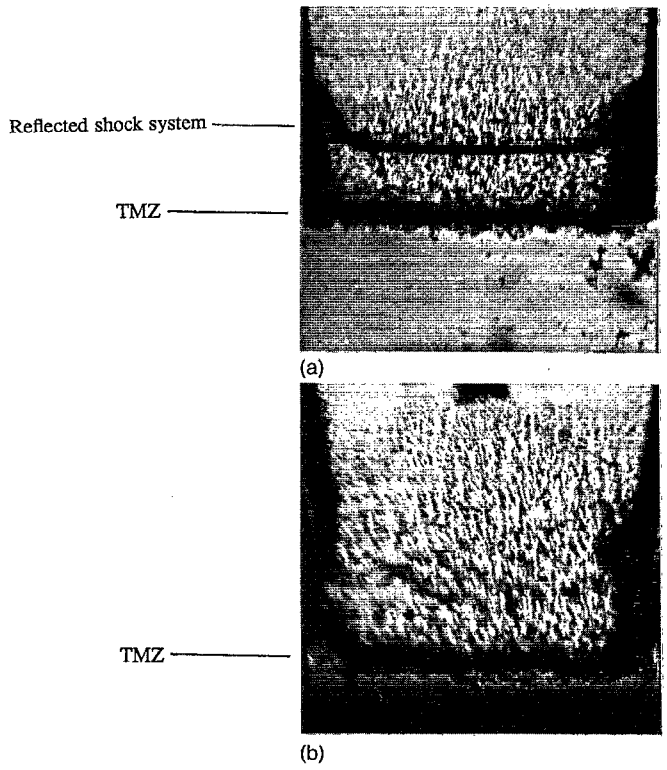

FIG. 13. Richtmyer–Meshkov instability of a plane discontinuous interface between air and helium. $M_s=1.32$, long period configuration. (a) $t=1.77$ msec, (b) $t=1.95$ msec.

a. Light–heavy interface. Figure 12 shows frames taken from a 35 000 fps motion picture of the same experimental run described in the wave diagram of Fig. 3. [The interface is shown just before the reshock in Fig. 8(b).] The first picture, at $t=4.39$ msec, shows the interface after the passage of the reflected shock. A "loop" or wall vortex, as first observed by Andronov *et al.*,[7] can also be distinguished on the side walls. It is caused by the interaction of the reflected shock with the distorted interface within the boundary layer and is a form of shock wave/boundary-layer interaction (cf. Brouillette[17]). A nonuniform acoustic field below the interface can also be noticed. These weak waves, seen reverberating between the side walls, originate from the scattering of the incident and reflected shocks at the distorted interface and boundary layer. This region appears very disturbed only because the high index of refraction of SF_6 makes the waves more visible to the schlieren system. The second picture, at $t=5.19$ msec, shows the interface still moving upward after the first reshock. Turbulence, generated and intensified by the interaction of the reflected wave with the already turbulent interface, has caused the thickness of the TMZ to increase. The wall vortex structure is even more visible at the side walls and also appears on the window as the gray region above the image of the interface. It is important to distinguish between the TMZ and the wall vortex when measuring the growth at the interface, as indicated in Figs. 12(a) and 12(b).

The time evolution of the thickness of the TMZ after the reshock for this experiment is shown in Fig. 9. It is seen that the interface is compressed noticeably by the reshock, and that thereafter the growth rate is 5.6 ± 0.6 m/sec.

b. Heavy–light interface. Figure 13 shows pictures obtained from a 60 000 fps high-speed schlieren motion picture of the interaction of a $M_s=1.32$ shock wave with an air/helium interface. The wave diagram of this run is shown in Fig. 4 and the interface before the reshock is shown in Fig. 10(b). At $t=1.71$ msec [Fig. 13(a)], the interface is shown instants after the interaction with the reflected shock, which is now seen just above the interface. Since the speed of sound in the helium–air boundary layer is much larger than in the air in the bulk of the fluid above the interface, precursor waves form on the side walls as the reshock crosses the interface. The turbulence intensity at the interface seems to have increased and the thickening of the TMZ can be noticed. Some 0.18 msec later [Fig. 13(b)], the interface still propagates toward the end of the tube. Its thickness has increased and larger scales have appeared on the interface. The extent of the boundary-layer region at the interface has also increased and could be affecting the development of the TMZ at this stage.

The time evolution of the TMZ after the reshock for this experiment is shown in Fig. 11. As opposed to the light–heavy interface, no interface compression is caused by the reshock; the latter induces a growth rate of 9.2 ± 1.4 m/sec of the TMZ.

Figures 14(a) and 14(b) compare the evolution of the air/He interface at two higher incident shock strengths. The qualitative features of the TMZ as well as the precur-

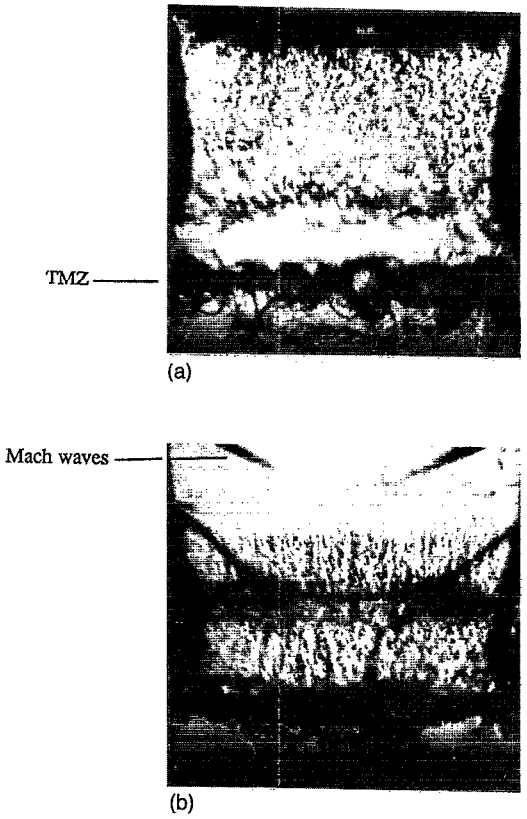

FIG. 14. Richtmyer–Meshkov instability of a plane discontinuous interface between air and helium, long period configuration. (a) $M_s=1.48$, $t=1.31$ msec; (b) $M_s=1.66$, $t=0.91$ msec.

sor waves are similar. In Fig. 14(a), for air/He $M_s=1.48$, the presence of large-scale structures in the TMZ is more apparent. This could validate the hypothesis that the entrainment mechanism at the interface involves the merging of small scales into larger ones. Two oblique waves can also be seen in Fig. 14(b) above the interface. These are Mach waves originating from small disturbances on the side walls of the test section upstream of the windows, because the flow velocity induced in air by the refraction of the incident shock at the interface is supersonic ($M=1.13$).

The parameters and measured growth rates for the discontinuous interfaces for long period experiments are given in Table I. It should be noted that for some of the long period experiments, the interaction of the reshock with the boundary layer at the interface is so violent that the interface cannot be distinguished from the wall vortex, making the measurement of the TMZ growth impossible. That is why some of the entries in Table I are missing.

C. Continuous interface

Since the sliding plate is used to separate the gases at the start of these experiments, only the light–heavy continuous interfaces are investigated. Perturbations on the continuous interface can be introduced by the pumping action of the retracting plate. However, since in most cases the large-scale perturbations are allowed to be damped out by letting the gases diffuse into each other for up to 6 sec, the

TABLE I. Experimental parameters—discontinuous interface—long period experiments.

			$d\delta/dt$ (m/sec) Wave 0			
Test gas	A_0	M_s	avg.	local	Wave 1	Run
He	−0.76	1.32	3.3	0.4	9.2	1213C
		1.48	5.1	0	30.4	1109A
		1.66	11.5	10.3	30.9	1214B
		1.66[a]	5.5	5.2		1208B
Air	0	1.32	0.9	0	0.5	1022C
		1.48	2.4	2.6	1.0	1024C
		1.66	3.6	5.3	4.1	1101B
R22	0.50	1.12	1.8	0.3	4.5	1210A
		1.32	3.4	0		1214C
		1.48	3.3	3.9		1213D
		1.66	3.2	0		1214A
SF_6	0.67	1.12	2.3	0	4.2	1018A
		1.32	2.3	1.0	5.6	1108C
		1.48	3.4	2.9		1104C
		1.66[a]	2.5	0		1111A

[a]Interface-window distance = 65 cm.

random small-scale perturbations possibly present on the interface are in the form of velocity and density fluctuations. When the initial thickness of the interface cannot be monitored before a run for the long period experiments, it is inferred from observations in the short period configuration and from concentration probe measurements.[17]

1. Growth after incident shock

Because the initial perturbations on the continuous interfaces are small and their thickness is large, their growth rate is expected to be very small.[27] It is observed experimentally that the growth induced by the arrival of the incident shock at the interface is negligible and that noticeable growth is measured only a long period after the arrival of the reverberations at the interface.

2. Growth after first reshock

The response of a continuous interface to the incident and first reflected wave is examined with experiments in the long period configuration. The wave diagrams for these runs are similar to those obtained with the discontinuous interfaces (e.g., Fig. 3).

Figure 15 shows schlieren photographs obtained from a 35 000 fps motion picture of an air/SF_6 interface initially accelerated by a $M_s=1.32$ shock. For this case the initial thickness δ_0 is assumed to be 30 mm. Figure 15(a) shows the interface 3.59 msec after the start of the interaction. Its measured thickness is reduced to $\delta=20$ mm because of compression by the incident shock and slow growth. The edges of the interface are curved upwards as a result of the influence of the developing boundary layer on the side walls. At $t=4.39$ msec [Fig. 15(b)], the interface is seen shortly after the reshock. Its thickness has been compressed again by the wave, but no turbulent growth is observed. The start of roll-up of a two-dimensional vortex structure can be noticed on the side walls, a manifestation

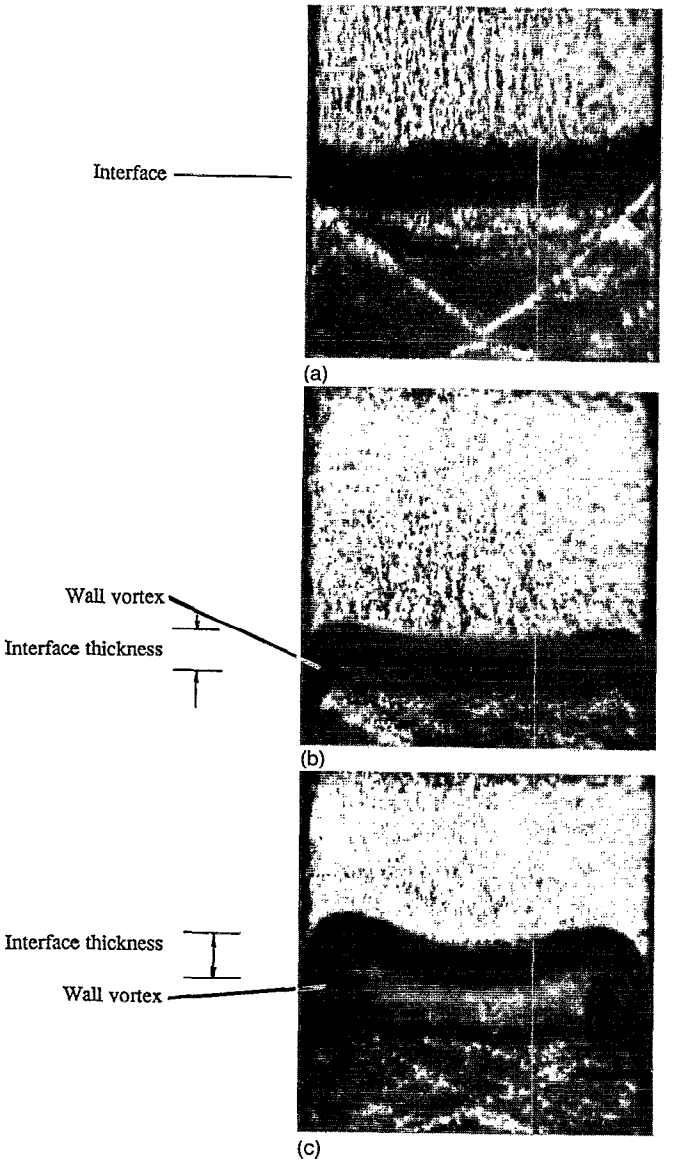

FIG. 15. Richtmyer–Meshkov instability of a plane continuous interface between air and SF_6. $M_s=1.32$, long period configuration. (a) $t=3.59$ msec, (b) $t=4.39$ msec, (c) $t=5.19$ msec.

of the shock/boundary-layer interaction at the interface. Figure 15(c) ($t=5.19$ msec) shows the wall vortex now fully developed, and its image on the observing window can clearly be seen below the interface. By this time, the vortices dominate the development of the interface. Stretching of the interface caused by the vortices could inhibit the turbulent spreading of the TMZ.

Figure 16 shows a plot of the evolution of the thickness of the interface. Before the first reflection, a local growth rate of 0.2 ± 0.1 m/sec is measured. The average growth rate from $t=0$ cannot be measured accurately, but an upper bound of 0.2 m/sec can be established. After the compression caused by the reshock, modest growth of 1.1 ± 0.3 m/sec is observed.

Table II lists the local incident shock and reshock growth rates for the long period continuous interface experiments. In addition, an upper bound to the average incident shock growth is presented. However, in most cases, the reshock growth rates cannot be obtained due to the violence of the shock wave/boundary-layer interaction which obscures the observation of the interface.

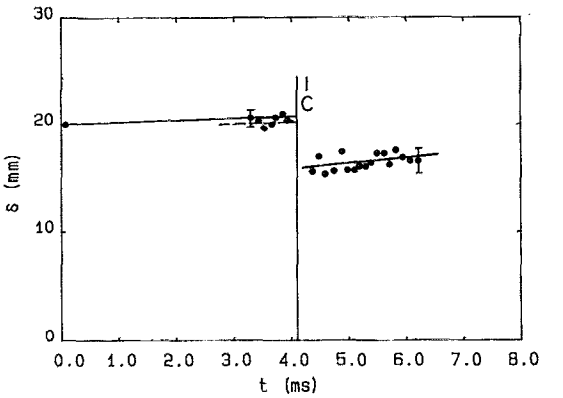

FIG. 16. Time evolution of the thickness of the plane continuous interface between air and SF_6. $M_s=1.32$, long period configuration. ——: upper bound to incident shock growth, reshock growth. – – –: local incident shock growth.

Note that at late times, as in Figs. 1, 12(b), and 15(c), the vortical structures at the walls are sufficiently large that the strain they induce on the interface near the center of the shock tube can make the interface thinner than it would otherwise be.

VI. DISCUSSION

A. Profile for incident TMZ growth

In the long period experiments with the discontinuous interface it has been noticed that the growth rate measured

TABLE II. Experimental parameters—continuous interface—long period experiments.

				$d\delta/dt$ (m/sec) Wave 0			
Test gas	A_0	M_s	δ_0' (mm)	avg.[a]	local	Wave 1	Run
R22	0.50	1.12	13	0.2	1.1		1122B
			29	0	0	0.2	1122A
		1.32	12	0.3	3.0		1123D
			26	0	1.0		1128A
		1.48	9	0.8	0.4		1129C
			9	1.2	0.2		1205A
			21	0	0.6		1202A
		1.66	10	0.8	4.2		1202C
			15	1.0	3.5		1202B
SF_6	0.67	1.12	15	0.2	0.1	4.8	1123A
			29	0	0		1123B
		1.32	11	0.2	0.5		1128B
			20	0.2	0.2	1.1	1128C
		1.48	9	1.8	2.3		1203A
			19	1.4	0		1203B
		1.66[b]	10	0.9	2.2		1206A
			17	0	7.2		1205B

[a]Upper bound.
[b]Interface-window distance=65 cm.

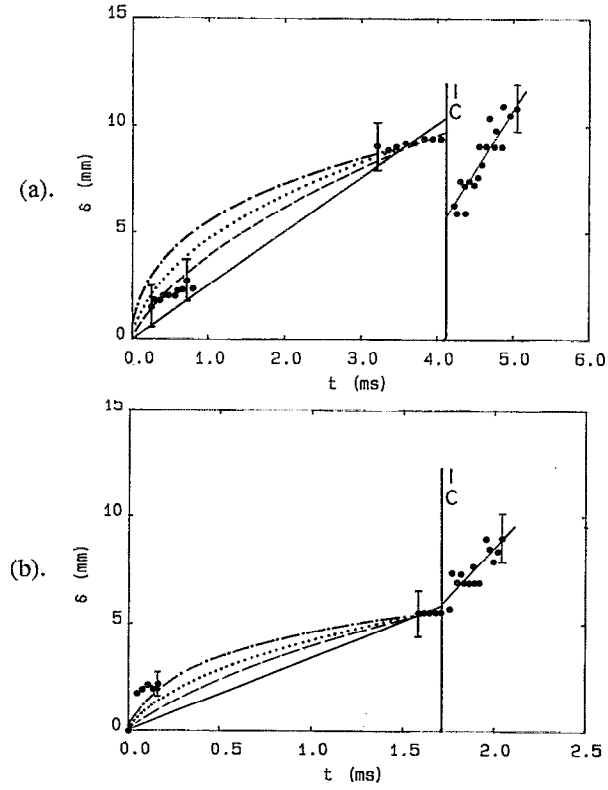

FIG. 17. Time evolution of the thickness of the TMZ for two discontinuous interface experiments. Long period and short period configurations. ——: linear profile ($\alpha=1$); – – –: $\alpha=2/3$; ···: $\alpha=1/2$; – · –: $\alpha=1/3$. (a) Air/SF_6 $M_s=1.32$; (b) Air/He $M_s=1.30$, 1.32.

while the TMZ is in the field of view of the observing window is almost always smaller than the average growth from $t=0$. Moreover, the upper bound to the incident shock growth in the short period configuration is usually larger than the average growth in the long period configuration. These observations indicate that the thickening of the interface slows down as time increases. This can be expected since, as discussed above, the nonlinear growth of a perturbation is always slower than its linear phase of development; furthermore, as turbulent mixing develops, the turbulence intensity decreases in time due to both the thickening of the interface, which spreads the energy over a larger volume, and viscous dissipation. In fact, using simple dimensional arguments, it was shown that the thickening of the interface follows a power law, i.e., $\delta \propto t^{\alpha}$, where $\alpha \leqslant 2/3$.

Thus, with the experimental results in both long period and short period configurations, it would seem to be possible to infer the power law governing the time evolution of the TMZ after interaction with the incident shock. Figures 17(a) and 17(b) show various power-law fits to the incident shock data from the TMZ plots of Figs. 9 and 11 for the discontinuous interfaces between air and SF_6 and air and helium, respectively, with $M_s=1.32$. It is seen that it is difficult to determine the exponent α with any accuracy because of the uncertainty in the data and the relative proximity of the various curves. The exponent can also be

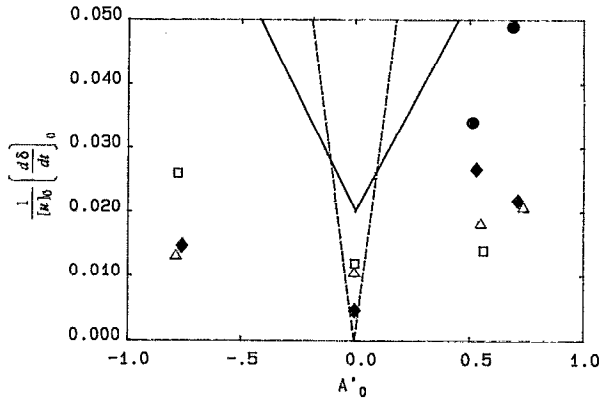

FIG. 18. Correlation of average incident shock growth rates for the discontinuous interface experiments in the long period configuration. Incident shock Mach number: ●: 1.12; ◆: 1.32; △: 1.48; □: 1.66. ——: Zaitsev *et al.*;[9] – – –: Mikaelian–Read formula.

obtained by straight-line least-squares fit of the incident shock data from both short period and long period experiments, plotted on a log–log scale. In this case, the rms error of the fit is compounded by the large relative error on the data points at the early times, and it is found that the exponent can achieve pretty much any value between 0 and 1, although the theoretical arguments presented above require that $\alpha \leqslant 2/3$.

B. Correlation of growth rate results

The results for the average growth rate after the incident shock of discontinuous interfaces in the long period configuration are correlated by plotting the growth rate $(d\delta/dt)_{0\,\mathrm{avg}}$ normalized by the velocity jump caused by the wave, $[u]_0$, as a function of postshock Atwood ratio A'_0. The results are presented in Fig. 18 for four incident shock Mach numbers and four gas combinations. The empirical correlation for similar experiments obtained by Zaitsev *et al.*[9] is also included in the plot along with the Mikaelian–Read[21] formula. The results of the present study clearly show smaller growth rates than those reported by Zaitsev *et al.*, although, with the longer interface–end-wall distance used in those experiments, their local growth rates should have been lower than those reported here. One can also see that the direct application of constant gravity Rayleigh–Taylor mixing results to the impulsive case is not adequate at all.

The results for the growth rate after the first reshock of discontinuous interfaces in the short period configuration are repeated here from Ref. 12. They were correlated by plotting the reshock growth rate $(d\delta/dt)_1$ normalized by the velocity jump caused by the wave, $[u]_1$, as a function of reshocked Atwood ratio A'_1. These results are presented in Fig. 19 for four incident shock Mach numbers and five gas combinations. The empirical correlation for a similar experiment obtained by Zaitsev *et al.*[9] is also included in the plot. In addition, the Mikaelian–Read formula is shown in the figure, with the added assumption that the incident shock does not induce any growth but only produces per-

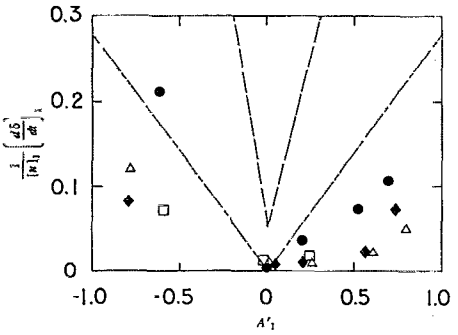

FIG. 19. Correlation of reshock shock growth rates for the discontinuous interface experiments in the short period configuration. Incident shock Mach number: ●: 1.12; ◆: 1.32; △: 1.48; □: 1.66. – –: Zaitsev *et al.*;[9] – – –: Mikaelian–Read formula. (From Fig. 11 of Ref. 12.)

turbations on the interface that are subsequently amplified by the first reshock. The present study again clearly shows smaller growth rates than those reported by Zaitsev *et al.*[9]

The results for the discontinuous interface shown in Fig. 19 for the reshock growth, and less markedly in Fig. 18 for the growth of the TMZ after the incident shock, exhibit a dependence on the strength of the shock not accounted for by the normalization: Relatively faster growth is observed for the weaker waves. This could be due to the higher compression produced by the stronger waves, which could have an inhibiting effect on the generation of turbulent energy at the interface. Moreover, since the initial perturbations at the interface are produced by the breaking of the membrane by the incident shock, the difference in strength of the waves could produce different perturbations. As was seen above in Eq. (1), the total kinetic energy E_k of the fluctuating motions caused by the baroclinic instability at the interface is strongly dependent on the properties of the initial perturbations. In fact, $E_k \propto \langle \eta^2 \rangle \bar{k}$, where $\langle \eta^2 \rangle$ is the spatial variance of the amplitude of the initial perturbation and $\bar{k}$ its average wave number. The variation in initial conditions could then be responsible for the decrease in growth rates. Because the energy available for the fluid motions is deposited at the interface only at the time of impulsive acceleration, the role played by the initial conditions on the subsequent entrainment between the two gases could be more important for the shocked case than for the constant-gravity case, where energy is continuously supplied to the flow. It is thus doubtful that the instability induced by the shocks at the plane interface achieves a regime of self-similar mixing that is independent of initial conditions.

We also note that the growth rate after incident shock is higher for $A_0' > 0$, i.e., for the light–heavy configuration, than for $A_0' < 0$. For $A_0' > 0$ the perturbations immediately begin to increase amplitude upon acceleration, while for $A_0' < 0$ the perturbations on the interface must first reverse phase before they grow. The opposite phenomenon is observed for the growth after the first reflected shock; it is noted that the reshock growth rate is higher for $A_1' < 0$, than for $A_1' > 0$. For the reflected shock, the perturbations immediately begin to increase amplitude upon reshock for $A_1' < 0$, while for $A_1' > 0$ the perturbations on the interface must first reverse phase before they grow. This is further evidenced by the fact that, for the light–heavy configuration, the TMZ seems compressed noticeably by the reshock (cf. Fig. 9), while for the heavy–light configuration very little compression is observed, as seen in Fig. 11. In addition, the fact that the incident shock accelerates interfaces with negative Atwood ratio to higher velocities than those with positive Atwood ratio might cause a more energetic pre-reshock state. If one or more of these effects are the cause of the above observations, it would again indicate that the reshock growth rate is sensitive to the initial pregrowth state of the interface.

On the other hand, a comparison of reshock growth rates for the discontinuous interface in both the long period experiments (Tables I and II) and short period experiments (Tables I and II of Ref. 12) does not uncover any particular trend. For the light–heavy interfaces, the reshock growth rates are larger for the short period experiments. The opposite is observed for the air/He interfaces, where faster growth is measured for the long period experiments. The interaction of the reshock with the interface increases the turbulent energy by two main mechanisms: One mechanism is the production of turbulent energy by baroclinic vorticity generation, as the shock interacts with the local density gradients present within the interface. If the turbulence at the interface is allowed to develop for a long period before the arrival of the reshock, then one would expect the density gradients to be reduced. Thus more turbulent energy would be created by the baroclinic instability if the interface interacts with the reshock just as it enters the nonlinear growth regime, when the amplitude of the perturbation is large and mixing has not started yet. The other mechanism involves the intensification of preexisting turbulence at the interface by shock-induced rapid distortion. In this case, it is generally agreed that the ratio of turbulent kinetic energy after the passage of the wave to that before is a function of shock compression. Since the turbulence intensity decreases as the TMZ thickness increases, more intensification would be achieved with a thin, thus more energetic, interface. These arguments seem to point out that reshock growth rates would be larger if the time delay before the reshock is smaller, as it has been observed for the light–heavy interfaces. It is not known why the opposite is observed for the air/He interfaces.

Figures 20 and 21 are attempts to correlate the growth rates of discontinuous interfaces in view of the above discussion. The growth rates after the incident shock are now normalized by the compression η_0'/η_0 (calculated from the 1-D gas-dynamics theory), as well as the velocity jump $[u]_0$ caused by the incident shock at the interface. The reshock growth rates are normalized by the sum of the absolute values of the velocity jumps induced by the incident shock and the first reflection. These results are further adjusted by dividing them by the total compression η_1'/η_0 produced by those first two waves. With these correlations, the results for positive and negative Atwood ratios seem to collapse reasonably well for both growth rate measurements.

In agreement with the results of Brouillette and

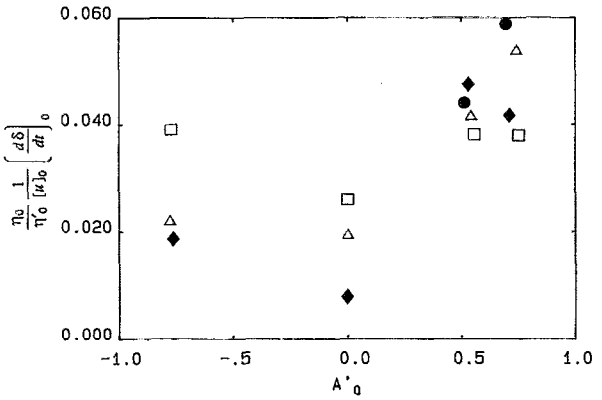

FIG. 20. Improved correlation of average incident shock growth rates for the discontinuous interface experiments in the long period configuration. Incident shock Mach number: ●: 1.12; ◆: 1.32; △: 1.48; □: 1.66.

Sturtevant,[27] perturbations on a thick interface grow much more slowly than on a discontinuous interface. Furthermore, the nonuniformities contained in the diffusively smoothed interfaces of the present experiments are probably small. Thus it is not surprising that each reverberation induces so little growth in the experiments with continuous interfaces and that growth is observed only after a long period delay.

C. Distinction between TMZ and wall vortex growth

Finally, to show the importance of using a flow visualization method capable of distinguishing between the wall vortex and the interface in the bulk of the fluid, we have repeated the experiment of Andronov *et al.*[7] for the turbulent thickening of a discontinuous air/He interface under multiple impulsive acceleration. In both the present and the Andronov experiment the strength of the incident shock was $M_s=1.30$ and the interface was initially 16.9 cm from the end wall of the test section. (Reference 12 has

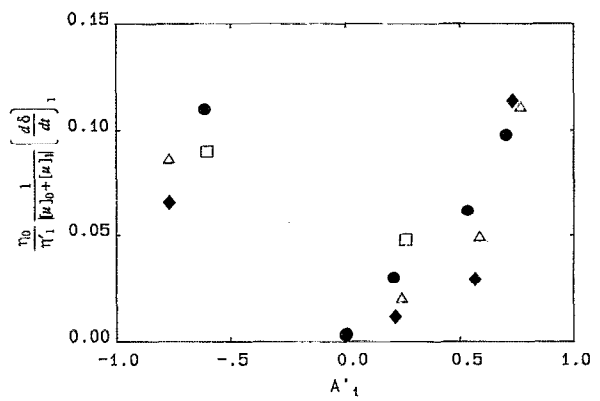

FIG. 21. Improved correlation of reshock shock growth rates for the discontinuous interface experiments in the short period configuration. Incident shock Mach number: ●: 1.12; ◆: 1.32; △: 1.48; □: 1.66. (From Fig. 16 of Ref. 12.)

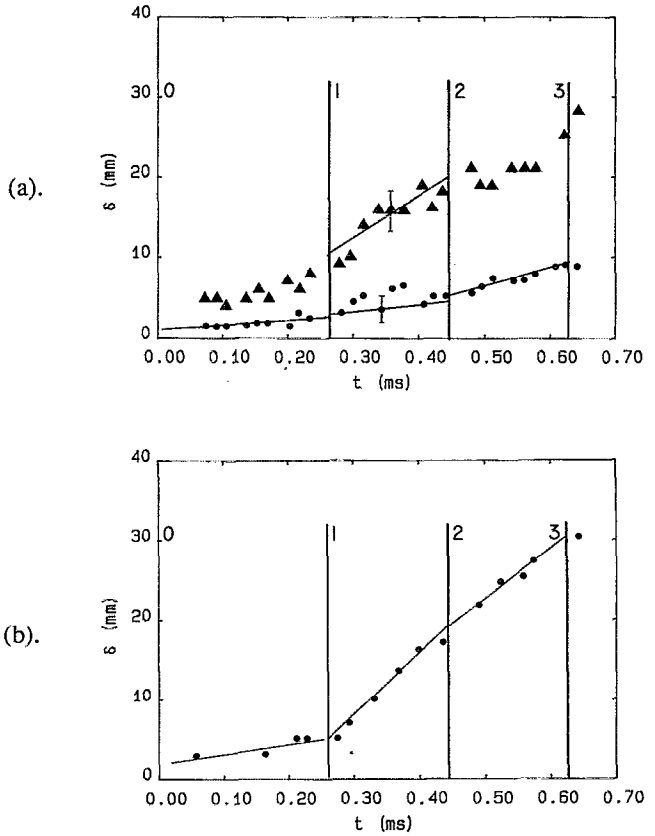

FIG. 22. Time evolution of the thickness of the interface for the plane discontinuous interface between air and helium. $M_s=1.30$. (a) Present study: ●: TMZ; ▲: wall vortex; (b) Andronov *et al.*:[7] ●: TMZ.

shown the results of a similar comparison with disparate geometries.) Figure 22(a) shows the time evolution for both the TMZ and the wall vortex in the present experiment. The reshock growth rate of the TMZ is 7.5 ± 1.2 m/sec and that of the TMZ is 49 ± 5 m/sec. For comparison, Fig. 22(b) shows, on the same scale, data obtained from Fig. 3 of Andronov *et al.*[7] The reshock growth rate is determined to be about 70 m/sec. There is better agreement for the wall vortex results of the present study and the TMZ growth measurement of Andronov *et al.* In the Andronov experiment the interface was formed by a 0.3–0.5 μm "organic film" and the test section was rectangular with dimensions 4 cm$\times$12 cm, as compared to 11.5 cm $\times$11.5 cm for the present study.

The disagreement between the present results and those of Zaitsev *et al.*[9] (Figs. 18 and 19) and Andronov *et al.*[7] (Fig. 22) could be attributed to a different interpretation of the data possibly due to the lack of distinction between the TMZ and the wall vortex in the Soviet experiments (although Andronov *et al.* had recognized the presence of the wall vortex or "loop" in their schlieren photographs). Other possibilities include differences between the schlieren systems used in each experiment, differences in geometries, and possible differences of the membrane thickness and composition, or some other, unknown, features of the experimental setups.

The influence of the wall vortex on the development of the interface in the bulk of the fluid cannot be overlooked. In particular, the volume of fluid entrained into the wall vortex is comparable to that within the TMZ after the reshock. We have shown[17] that the wall vortices reduce the growth rate of the TMZ by stretching the latter, and that the magnitude of this effect is comparable to the TMZ growth rates for the slow-thickening continuous interfaces. This effect is amplified as the size of the shock tube test section is reduced.

VII. CONCLUSIONS

The experiments reported in this paper have elucidated the physical processes taking place when one, two, or many shock waves interact with a plane interface separating two gases of different densities. For the discontinuous interface formed by a thin plastic membrane, the perturbations on the interface are introduced by the rupture of the membrane and it is found that they evolve rapidly into the nonlinear turbulent mixing regime. Comparatively more growth is observed for the light–heavy than for the heavy–light interfaces since the latter have to undergo a phase reversal before they grow. Experiments performed in two different configurations have allowed the observation of the incident shock growth over a long time period and a slowdown of the thickening rate of the interface was shown to take place. However, the proximity of each power law and the large uncertainty in the data at the early times prevents the accurate determination of a possible universal power law describing the time evolution of shocked interfaces. Results for the reshock growth rates of these interfaces show that a noticeable increase of the turbulence intensity can be caused by the interaction of a shock wave with an already turbulent interface. It is seen that comparatively lower growth rates are induced by the stronger waves because they produce a larger compression of the perturbations. For some experiments, the entrainment process at the interface has been shown to be dominated by the evolution of large-scale structures. Both incident shock and reshock growth rate results are nearly an order of magnitude smaller than those observed by other investigators for similar experiments.

Experiments with continuous interfaces have demonstrated that a dramatic reduction in the growth of a possible turbulent mixing zone can be achieved by reducing the density gradient at the interface. These interfaces exhibit growth only at late times, after the development of perturbations introduced by the reverberation of waves between the end wall, the side walls, and the distorted interface under the influence of boundary layers. The vortical structures created by the shock wave/boundary-layer interaction on the edges of the interface induce strain that would effectively reduce the turbulent spreading of the interface and impair the observation of interface phenomena in the bulk of the fluid.

ACKNOWLEDGMENTS

This research was supported by the U.S. Department of Energy, Lawrence Livermore National Laboratory, under project agreement DOE W-7405-ENG-48.

[1] R. D. Richtmyer, "Taylor instability in shock acceleration of compressible fluids," Commun. Pure Appl. Math. **8**, 297 (1960).

[2] E. E. Meshkov, "Instability of the interface of two gases accelerated by a shock wave," Sov. Fluid Dyn. **4**, 101 (1969).

[3] F. E. Marble, G. J. Hendricks, and E. E. Zukoski, "Progress toward shock enhancement of supersonic combustion processes," AIAA Paper No. 87-1880, 1987.

[4] I. Waitz, F. E. Marble, and E. E. Zukoski, "An investigation of a contoured injector for hypervelocity mixing augmentation," AIAA Paper No. 91-2265, 1991.

[5] J. D. Lindl and W. C. Mead, "Two-dimensional simulation of fluid instabilities in laser fusion pellets," Phys. Rev. Lett. **34**, 1273 (1975).

[6] Yu. F. Afanas'ev, N. G. Basov, E. G. Gamalii, O. N. Krokhin, and V. B. Rosanov, "Symmetry and stability of laser-driven compression thermonuclear targets," JETP Lett. **23**, 566 (1976).

[7] V. A. Andronov, S. M. Bakhrakh, E. E. Meshkov, V. N. Mokhov, V. V. Nikiforov, A. V. Pevnitskii, and A. I. Tolshmyakhov, "Turbulent mixing at contact surface accelerated by shock wave," Sov. Phys. JETP **44**, 424 (1976).

[8] V. A. Andronov, S. M. Bakhrakh, E. E. Meshkov, V. V. Nikiforov, A. V. Pevnitskii, and A. I. Tolshmyakhov, "An experimental investigation and numerical modeling of turbulent mixing in one-dimensional flows," Sov. Phys. Dokl. **27**, 393 (1982).

[9] S. V. Zaitsev, E. V. Lazareva, V. V. Chernukha, and V. M. Belyaev, "An experimental investigation and numerical modeling of turbulent mixing in one-dimensional flows," Sov. Phys. Dokl. **30**, 579 (1985).

[10] G. Rodriguez, "Réalisation d'un Tube à Choc et Visualisation d'une Interface Gaz–Gaz par Strioscopie," Mémoire d'Ingénieur, CNAM, Paris, 1989.

[11] R. F. Benjamin, "Experimental observations of shock stability and shock-induced turbulence," in *Proceedings of the International Workshop on the Physics of Compressible Mixing, Princeton, 1988*, Lecture Notes in Engineering (Springer-Verlag, Berlin, 1990), p. 89.

[12] M. Brouillette and B. Sturtevant, "Growth induced by multiple shock waves normally incident on plane gaseous interfaces," Physica D **37**, 248 (1989).

[13] K. O. Mikaelian, "Simulation of the Richtmyer–Meshkov instability and turbulent mixing in shock-tube experiments" (private communication, 1985).

[14] B. Sturtevant, "Rayleigh–Taylor instability in compressible fluids," in *Shock Tubes and Waves*, edited by H. Grönig (VCH, Wendeim, Germany, 1988), p. 89.

[15] P. G. Saffman and D. I. Meiron, "Kinetic energy generated by the incompressible Richtmyer–Meshkov instability in a continuously stratified fluid," Phys. Fluids A **1**, 1767 (1989).

[16] K. I. Read, "Experimental investigation of turbulent mixing in Rayleigh–Taylor instability," Physica D **12**, 45 (1984).

[17] M. Brouillette, "On the interaction of shock waves with contact surfaces between gases of different densities," Ph.D. thesis, California Institute of Technology, 1989.

[18] G. I. Barenblatt, "Self-similar turbulence propagation from an instantaneous point source," in *Non-Linear Dynamics and Turbulence*, edited by G. I. Barenblatt, G. Ioos, and D. D. Joseph (Pitman, Boston, 1983), p. 48.

[19] C. E. Leith, "Development of a two-equation turbulent mix model," Lawrence Livermore Laboratory Report No. UCRL-96036, 1986.

[20] S. Gauthier and M. Bonnet, "A k-ϵ model for turbulent mixing in shock-tube flows induced by Rayleigh–Taylor instability," Phys. Fluids A **2**, 1685 (1990).

[21] K. O. Mikaelian, "Turbulent mixing generated by Rayleigh–Taylor and Richtmyer–Meshkov instabilities," Lawrence Livermore Laboratory Report No. UCRL-93499, 1985.

[22] G. I. Taylor, "The instability of liquid surfaces when accelerated in a direction perpendicular to their planes, I.," Proc. R. Soc. London Ser. A **201**, 192 (1950).

[23] J. C. R. Hunt, "A review of the theory of rapidly distorted turbulent flows and its application," Fluid Dyn. Trans. **9**, 121 (1978).

[24]C.-T. Wu, J. H. Ferziger, and D. R. Chapman, "Simulation and modeling of homogeneous compressed turbulence," NASA-CR-176939, 1985.
[25]L. Hesselink and B. Sturtevant, "Propagation of weak shock waves through a random media," J. Fluid Mech. **196**, 513 (1988).
[26]H. Mark, "The interaction of a reflected shock wave with the boundary layer in a shock tube," J. Aero. Sci. **24**, 304 (1957).
[27]M. Brouillette and B. Sturtevant, "Experiments on the Richtmyer–Meshkov instability: Single-scale perturbations on a continuous interface," submitted to J. Fluid Mech.